Effect of frictional heating and thermal advection on pre-seismic sliding: A numerical simulation using a rate-, state- and temperature-dependent friction law

Salvatore de Lorenzo, Mariano Loddo

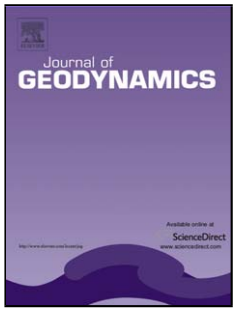

Title: Effect of frictional heating and thermal advection on pre-seismic sliding: A numerical simulation using a rate-, state- and temperature-dependent friction law

Authors: Salvatore de Lorenzo, Mariano Loddo

PII: S0264-3707(09)00063-5
DOI: doi:10.1016/j.jog.2009.07.001
Reference: GEOD 890

To appear in: *Journal of Geodynamics*

Received date: 15-6-2009
Revised date: 19-7-2009
Accepted date: 22-7-2009

Please cite this article as: de Lorenzo, S., Loddo, M., Effect of frictional heating and thermal advection on pre-seismic sliding: A numerical simulation using a rate-, state- and temperature-dependent friction law, *Journal of Geodynamics* (2008), doi:10.1016/j.jog.2009.07.001

Effect of frictional heating and thermal advection on pre-seismic sliding: a numerical simulation using a rate-, state- and temperature-dependent friction law

Salvatore de Lorenzo and Mariano Loddo

Dipartimento di Geologia e Geofisica and Centro Interdipartimentale Rischio Sismico e Vulcanico - Università di Bari, Italy

ABSTRACT

Laboratory experiments on simulated faults in rocks clearly show the temperature dependence of **dynamic** rock friction. Since rocks surrounding faults are permeable, we have developed a numerical method to describe the thermo-mechanical evolution of the pre-seismic sliding phase which takes into account both the rate-, state- and temperature-dependent friction law and the heat advection term in the energy equation. We consider a laminar fluid motion perpendicular to **a vertical** fault plane and assume that fluids move away from the fault plane. A semi-analytical temperature solution which accounts for the variability of slip velocity and stress on the fault has been found. This solution has been generalized to the case of a time varying fluid velocity and then was used to include the thermal pressurization effect. After discretizing the temperature solution, the evolution of the system is obtained by the solution of a system of first order differential equations which allows us to determine the evolution of slip, slip rate, friction coefficient, effective normal stress, temperature and fluid velocity. The numerical solutions are found using a Runge-Kutta method with an adaptative stepsize control in time. When the thermal pressurization effects can be neglected, the heat advection effect gives rise to a delay, with respect to the purely conductive case, of the earthquake occurrence time. This delay increases with increasing permeability H of the system. When the thermal pressurization effects are taken into account the situation is opposite, i.e. the onset of instability tends to precede that of the purely conductive case. The advance in the time of occurrence of instability increases with increasing coefficient of thermal pressurization. In the small permeability range ($H \leq 10^{-18}$ m^2), the seismic moment and nucleation length of the pre-seismic phase are significantly smaller than those predicted by the purely conductive model.

INTRODUCTION

Many studies have concerned aseismic slip on faults before an earthquake (e.g. Lockner and Byerlee, 1995 and references therein). Laboratory and theoretical studies of the mechanical

evolution of a fault during the earthquake seismic cycle show that a significant amount of slip could be generated before the unstable sliding phase, causing an degree of crustal deformation that could be measured by modern instruments (Lorenzetti and Tullis, 1989). Although seismic risk studies are actually in a very early stage, this aspect is very important for future studies aimed at determining possible precursors of earthquake instability (e.g. Dieterich, 1992). For this reason, several studies have been dedicated to the development of predictive models of the pre-seismic sliding phase (Kato, 2001 and references therein).

In describing the dynamical evolution of a fault, the seismic cycle is usually modelled considering the formal analogy with an elastic system comprising an elastic spring connected to a rigid block and assuming a constitutive friction law derived from laboratory studies. In earlier works, Dieterich (1979) and Ruina (1983) found a rate- and state- dependent friction law to explain a large amount of laboratory data on rock friction. These relations, which constitute the basis of all the subsequent studies of the seismic cycle, have been further improved to incorporate the effect of temperature variations on the friction coefficient (Chester and Higgs 1992; Blanpied *et al*. 1998; Hirose and Shimamoto 2005; Di Toro *et al*. 2006; Beeler *et al*. 2007).

Starting from the pioneering work of McKenzie and Brune (1972), many kinematical and dynamical approaches have been developed to obtain detailed models of the temperature distribution due to the frictional heating along a fault and around it (e.g.: Cardwell *et al*. 1978; Fialko 2004; Caggianelli *et al*. 2005 and references therein). In all these studies the thermal evolution is inferred by considering only the conduction term in the energy equation, without accounting for the heat transport related to fluid movement through the permeable rocks.

It is well known that purely conductive heat models are actually unable to explain heat flow data recorded in the proximity of faults. One of the most debated questions is, in fact, the so-called *heat flux paradox*, namely the discrepancy between the high heat fluxes predicted by theoretical conductive models and the small values of heat flux measured immediately after the earthquakes along the S. Andreas fault (e.g. Lachenbruch 1980). The possible reasons for this discrepancy have been largely debated in seismological literature. In particular, Madariaga (2007) has summarized the main results of the on-going researches and pointed out the need of taking into account the role of fluids along the faults. Sibson (1973) observed that if fluids are present in interconnected pores in the fault zone, the frictional heating could increase the fluid pressure, causing a reduction of the effective normal stress on the fault plane and favoring slipping along it. Starting from this observation, many studies (e.g. Lachenbruch 1980; Mase and Smith 1987; Bizzarri and Cocco 2006A, 2006B; Rice 2006) have focused on the effect of frictional heating and pore fluid pressure during the coseismic stage. In addition, Segall and Rice (2006) have analyzed the conditions for

which the shear heating effect on pore fluid can contribute to the nucleation phase. However, with the exception of the article of Mase and Smith (1987), where the heat advection term is included in the energy equation, in all other studies the heat equation is usually decoupled from the fluid pressure equation, by neglecting the heat advection term in the energy equation. This is because, as argued by Lachenbruch (1980), if we consider the small values of permeability of the fault core (< 10^{-17} m^2), the effect of heat advection can be considered negligible in the coseismic time interval (seconds or tens of seconds). A commonly accepted model of a fault zone (e.g. **Sibson 2003**) consists in fact of a thin fault core, having a small permeability, embedded in a much broader fractured zone, called the damage zone (**Chester and Chester 1998**) and having a greater permeability.

As concerns the fault core, even if some studies (Scholz, 1990 and references therein) suggest that the fault core has a thickness of the order of several millimeters or centimeters, the validity of the above simplified assumption is approximately maintained if the average properties of the fault core are considered in the modeling of the slip along the fault plane. As we will discuss in the following, this is particularly true in the case of the description of the pre-seismic sliding phase which involves long time scales, in the order of several hundred of days.

As concerns the permeability, at present there is no general agreement on permeability values around the fault zone. In some cases (e.g. Cappa *et al*. 2005, 2007) a higher permeability (from 10^{-12} to 10^{-8} m^2) has been inferred inside the damage zone, whereas in other studies (e.g. Wibberley and Shimamoto 2003) a smaller permeability has been estimated in this zone (from 10^{-15} to 10^{-18} m^2). Moreover, results of many studies (e.g. Noir *et al*. 1997; Miller *et al*. 2004; Antonioli *et al.* 2005) indicate that the average permeability inferred from seismological investigations may be, in some cases, eight orders of magnitude greater (until to 10^{-8} m^2) than the laboratory estimates on cataclastic rocks. An increase of permeability in the neighborhood of the fault plane in respect to the permeability values measured in laboratory experiments has been also predicted (Scholz 2002; Andrews 2005).

Based on these considerations, in this article, starting from the conductive model of Kato (2001), we present a thermo-mechanical model of the seismic cycle which incorporates the effect of both heat conduction and heat advection. To allow for an analytical formulation of temperature, we assume that fluids move perpendicularly to the fault plane. An analytical solution to the heat advection-conduction problem is presented for the case where slip velocity and shear stress are constants. By following the approach proposed by Kato (2001), this solution is generalized to the case where slip velocity and shear stress are allowed to vary over the time.

To account for the thermal pressurization effect we consider the hydro-dynamical model, named model II, in Segall and Rice (2006).

The results have been compared with the simulation results of Kato (2001) to evaluate how the advection and pressurization effects modify both the slip during the preseismic phase and the recurrence time of the earthquakes.

2. THEORY

2.1 THE RATE-, STATE- AND TEMPERATURE- DEPENDENT FRICTION LAW

Following Kato (2001), we consider a **single** spring-block model to simulate pre-seismic sliding on a planar surface (Fig.1). The fault plane is represented by the interface between the base of the rigid block and the floor. The spring simulates the elastic medium surrounding the fault. In the quasi-static approximation (Belardinelli *et al*. 2003 and references therein) the relationship between the shear stress acting on the base of the rigid block and its displacement is given by:

$$\tau = k(u_0 - u), \qquad (1)$$

where k is the spring stiffness, u_0 is the load-point displacement and u is the displacement of the rigid block. The shear stress τ is related to the effective normal stress by the equation:

$$\tau = \mu\sigma_n^{eff}, \qquad (2)$$

where μ is the friction coefficient.

Starting from the early works of Dieterich (1979) and Ruina (1983), which inferred the fundamental rate- and state- constitutive equations of **dynamic** rock friction **at low velocity and at a constant effective normal stress**, several laboratory studies have investigated the dependence of the friction coefficient on slip velocity and temperature. In what follows we use the rate-, state- and temperature-dependent friction law derived from Chester (1994) (see also Blanpied *et al*. 1995, 1998) and summarized in Kato (2001):

$$\mu = \mu_0 + a\left[\ln\left(\frac{V_s}{V_s^*}\right) + \frac{Q_a}{R}\left(\frac{1}{T} - \frac{1}{T^*}\right)\right] + b\theta \qquad (3)$$

In equation (3) R is the universal gas constant, T is the absolute temperature, Q_a is an apparent activation energy, $V_s = \frac{du}{dt}$ is the sliding velocity of the block, μ_0 is the value assumed by the friction coefficient for $V_s = V_s^*$ and T=T*; a and b are constants representing the time dependent property of friction; T*=T(t=0) is a reference temperature and $V_s^* = V_s\left(T = T^*\right)$.

The state variable θ quantifies the contact state between sliding surfaces or the internal structure of the gouge layer between sliding surfaces, and its evolution with time is expressed by the so-called slip law (Chester 1994, 1995):

$$\frac{d\theta}{dt} = -\frac{V_s}{L}\left[\theta + \ln\left(\frac{V_s}{V_s^*}\right) + \frac{Q_b}{R}\left(\frac{1}{T} - \frac{1}{T^*}\right)\right] \qquad (4)$$

In equation (4) Q_b is an apparent activation energy and L is the characteristic length controlling the evolution of the state variable (Bizzarri and Cocco 2003). In a study of the slip-weakening behavior of rate- and state- dependent constitutive laws, Cocco and Bizzarri (2002) found that the slip weakening curve displays an equivalent slip-weakening distance D_0^{eq} which is different from L. They showed that a scaling relation between D_0^{eq} and L exists such that $D_0^{eq}/L \approx 15$. Moreover, they discovered a difference between laboratory estimates of the parameter L (of the order of 1÷10 μm) and those (of the order of 1÷5 cm) derived from strong motion recordings. Based on these findings, we decided to use L=1 cm in our simulations. In the most general case the state variable will vary during the pre-seismic sliding phase, requiring to solve a system in the unknowns τ, V_s, θ and T. **To simplify the approach to the numerical solution and to obtain results comparable with those of Kato (2001) we consider the simplified case where the state variable θ is in the steady steate $\frac{d\theta}{dt} = 0$. In this case, following Kato (2001), we use** the steady state friction coefficient μ_{ss} defined as $\mu_{ss} = \mu\left(\frac{d\theta}{dt} = 0\right)$. From equation (3) and (4) it immediately follows that:

$$\mu_{ss} = \mu_0 + (a-b)\ln\left(\frac{V_s}{V_s^*}\right) + \frac{aQ_a - bQ_b}{R}\left(\frac{1}{T} - \frac{1}{T^*}\right) \qquad (5)$$

The time derivative of equation (1) gives:

$$\frac{d\tau}{dt} = k(V_0 - V_s), \qquad (6)$$

where $V_0 = \frac{du_0}{dt}$ is the load point velocity. By combining (2), (3), (4) and (5), Kato (2001) obtained:

$$\frac{d\tau}{dt} = \sigma_n^{eff}\left[\frac{a}{V_s}\frac{dV_s}{dt} + a\frac{Q_a}{R}\frac{dT^{-1}}{dt} - \frac{V_s}{L}(\mu - \mu_{ss})\right] \qquad (7)$$

The rate and state friction laws have been validated in laboratory stick-slip experiments in which the slip velocity varies approximately in the range $10^{-6}<V_s<10^{-1}$ m/s (Mair and Marone, 1999)

2.2 THE COUPLING BETWEEN TEMPERATURE AND FLUID PRESSURE

Equation (6) and (7) indicate that the mechanical evolution of the spring-block system depends on the time derivative of the temperature on the sliding surface. Kato (2001) considered the case of a natural system where the temperature evolution is governed only by heat conduction. He reformulated the problem, previously solved by McKenzie and Brune (1972), to incorporate the time dependence of the slip velocity and the shear stress. In what follows, we consider the case of a natural system where the heat is transferred not only by conduction but also by fluid advection. The volumetric flow rate per unit area q can be obtained from the fluid pressure gradient ∇p using the Darcy's law (e.g. Turcotte and Schubert, 1982):

$$q = -\frac{H}{\gamma}\nabla p\,, \qquad (8)$$

where H is the permeability of the fault-rock system and γ the dynamical viscosity of fluids. The volumetric flow rate q has the dimension of a velocity (and therefore it is also named Darcy's velocity) and expresses the average velocity per unit area and not the fluid particle velocity (Guéguen *et al.* 1997; Bizzarri and Cocco 2006A). Fluid velocity v can be inferred from q using the equation (e.g. Miller *et al*. 2004 and references therein):

$$v = \frac{q}{\phi} \qquad (9)$$

where ϕ is the porosity of rocks.

In the most general case of a 3D medium, fluids through the permeable rock matrix move both in the direction perpendicular to the fault plane and along it. Many authors (Lachenbruch 1980; Mase and Smith 1987; Bizzarri and Cocco 2006A; Segall and Rice 2006 among the others) have considered only the component of the fluid velocity perpendicular to the fault plane. This approximation makes it possible to obtain a mathematical description of the effect of increase of pore pressure perpendicularly to the fault plane due to the increase of temperature near the fault plane and corresponds to the case of a laminar fluid motion related to fluid pressurization (i.e. one dimensional Darcy flow perpendicular to the fault plane), as described in Bizzarri and Cocco (2006A). In what follows we will approximate fluid motion as laminar fluid motion. As we will show, this assumption will allow us to obtain a system of first-order differential equations which can be numerically managed without a prohibitive computational effort.

In particular, to quantify how the temperature variations modify the pore fluid pressure (and therefore the fluid velocity) we have considered the transport model described in Segall and Rice (2006). This model treats the thermal and hydraulic properties as homogeneous and takes the limit

of zero fault zone thickness, which is the case considered in this article. Under these conditions, the relation between fluid pressure and temperature on the fault plane is given by (Mase and Smith 1987; Segall and Rice 2006):

$$p - p^* = \frac{\Gamma\left(T - T^*\right)}{1 + \sqrt{\frac{c_{hyd}}{\eta}}} \approx \Gamma\left(T - T^*\right) \tag{10}$$

where the last equality arises because the hydraulic diffusivity of water c_{hyd} is usually at least an order of magnitude smaller than the thermal diffusivity η. In equation (10) p^* is the pressure at the background temperature $T=T^*$ and **Γ is the thermal pressurization factor, defined as the ratio between the fluid volume expansion due to a unit increase in temperature and the fluid volume expansion due a unit decrease in fluid pressure (for a detailed discussions on the values of Γ in different fluid regimes the reader is referred to Mase and Smith, 1987).** In particular, Γ depends on the compressibility β, the pressure and the temperature of the rocks surrounding the fault (Mase and Smith 1987). For values of β smaller than the compressibility of the water ($\beta \approx 10^{-10}$ Pa^{-1}), Γ ranges from 0.6 MPa K^{-1} and 1.1 MPa K^{-1} (Segall and Rice 2006). For high values of compressibility ($\beta \approx 10^{-6}$ Pa^{-1}), Γ can be smaller than 0.01 MPa K^{-1} in the whole temperature range of the solid rocks at high pressures (>100 MPa) (Mase and Smith 1987), so that the effect of thermal pressurization becomes negligible. In this particular case, fluid velocity maintains constant and it is then possible to neglect the thermal pressurization effect.

2.3 THE TEMPERATURE EVOLUTION IN THE CASE OF A CONSTANT FLUID VELOCITY

We have built a physical model which replicates the **main** features of the fluid dynamics around a fault. In the most general case fluids inside the fault core tend to move along the direction of the pressure gradient. For this reason we assume that the pressure gradient is orthogonal to the fault plane and that the fluids in the fault core move perpendicularly to the fault plane with a geometrically averaged velocity v. Moreover, to allow for an analytical approach we assume that fluid motion does not have a component in the direction of the fault plane. **More sophisticated 2D numerical solutions for the fluid- and thermo- dynamical problem have been developed by Williams and Narasimhan (1989) for the study of the San Andreas fault and by Goyal and Narasimhan (1982) for the case of a fault-controlled geothermal reservoir charged at a constant pressure (1982). However these equations do not incorporate the effect of rate-, state- and temperature- dependent friction laws. In particular, in the case of San Andreas fault, Williams and Narasimhan (1989) pointed out that the topography associated with the fault**

zone may be the key to a final understanding of the state of stress along the fault. They conclude that the topography may bound a low stress fault with low permeability and high pore pressure gouge, or, alternatively, the topography may serve as a cause of gravity induced fluid flow away from high stress fault characterized by fractured, permeable gouge. The importance of accounting for both the pore fluid pressure and the aseismic slip, in the frame of the rate and state approach, at the San Andreas fault, has been underlined also by Scholz (1998). He pointed out the existence of a 170 km long creeping section of the San Andreas fault where the fault slip aseismically, in the conditionally stable regime of the rate- and state-friction law. He attributed the anomalous behaviour of this section of the fault to the presence of unusually high pore pressures in the fault zone.

It is worth noting that, as a consequence of our choice of considering a fluid motion perpendicular to the fault plane, the effect of cooling of the fault plane is maximized, in that, in this case, heat is transported away from the fault more rapidly than in the case of a fluid motion having a component parallel to the fault plane. Finally, the developed solution refers only to the case of a vertical fault plane (fig. 1), since only in this case we can assume the symmetry of the thermo-mechanical solutions with respect to both the sides of the fault plane.

The effect of a finite shear zone on the thermo-mechanical evolution of the system has been the subject of several studies (Lachenbruch, 1980; Fialko, 2004; Rice, 2006 among the others). All these studies are in agreement as concerns the reduction of the maximum temperature rise in the fault zone with increasing the fault zone thickness. In particular, Lachenbruch (1980) observed that an initially broad shear zone would tend to contract about the plane where the initial strain rate (and consequently, heat production, temperature, and fluid pressure rise) happened to be greatest. He also pointed out the role of fluid pressure in the narrowing of a fault zone. Moreover, worldwide evidence exists for very thin shear zones in the Earth. Rice (2006) summarized the results of recent field observations and suggested that slip in individual earthquakes may be extremely localized and occurs primarily within a thin shear zone, <1–5 mm thick. The localized shear zone lies within a finely granulated (ultracataclastic) fault core of typically tens to hundreds millimeter thickness, that core itself fitting within a much broader damage zone of granulated or incompletely cracked rock (Rice, 2006). Interestingly, Rice (2006) showed that to avoid melting on the shear zone of the Punchbowl fault of the San Andreas fault system, its thickness should be at least 35 mm or higher, whereas field observations and laboratory data clearly indicate that the thickness of this shear zone is in the order of 1 mm. Therefore fluid pressure could be invoked to reduce the shear

stress on a thinner fault and thus avoid the melting. This, or some other weakening mechanism, has to occur along faults where pseudotachylytes are not observed.

Accordingly, we consider the limit situation where the fault core thickness tends to zero and reduces to a fault plane located in z=0. (Fig. 1).

We first consider the case of a constant average fluid velocity in the fault core.

In the 1D case the equation governing the heat redistribution is (e.g. Lachenbruch, 1980):

$$\eta_{sf}\frac{\partial^2 T}{\partial z^2}-\frac{(\rho_w C_w)}{(\rho C)_{sf}}v\frac{\partial T}{\partial z}=\frac{\partial T}{\partial t} \qquad (11)$$

In equation (11) η_{sf} is the thermal diffusivity of the solid-fluid compound, ρ_w and C_w are, respectively, the density and the specific heat at constant pressure of the fluid phase, $(\rho C)_{sf}$ is the heat capacity for unit volume of the solid-fluid compound and z is the distance from the sliding surface. η_{sf} and $(\rho C)_{sf}$ are related by the equation (e.g. Lachenbruch, 1980):

$$\eta_{sf}=\frac{K_{sf}}{(\rho C)_{sf}} \qquad (12)$$

where K_{sf} is the thermal conductivity of the solid-fluid compound. Following Mase and Smith (1987) we compute K_{sf} as:

$$K_{sf}=K_s^{1-\phi}K_w^{\phi} \qquad (13)$$

where K_s and K_w are the thermal conductivity of the solid and fluid phase respectively and ϕ is the porosity. Moreover:

$$(\rho C)_{sf}=\rho_s C_s(1-\phi)+\rho_w C_w\phi \qquad (14)$$

where ρ_s and C_s are the density and the specific heat at constant pressure of the solid phase respectively.

As an effect of a relative slip *ds* of the two blocks respect to the fault plane, the work $d\Omega$ done by the frictional force is converted into heat *dQ*:

$$dQ=d\Omega=\tau A ds \qquad (15)$$

where *A* is the surface of the blocks in contact. Therefore the fault surface acts as a heat source which produces a heat flux quantity $\Phi(z=0,t)$ given by:

$$\Phi(z=0,t)=\frac{1}{A}\frac{dQ}{dt}=V_s(t)\tau(t) \qquad (16)$$

The heat production term given by equation (16) can therefore be included in the energy equation (11) as a boundary condition. In fact, in an infinite medium the heat flux splits in two equal contributions, so that in the half-space z>0 the boundary condition (16) gives rise to:

$$\left[-K_{sf}\frac{\partial T}{\partial z}+\rho_w C_w v T\right]_{z=0}=\frac{V_s(t)\tau(t)}{2} \tag{17}$$

where the first term in the square parenthesis is the conductive heat flux and the second term is the advective heat flux (e.g. Incropera and DeWitt, 1996).

The analytical solution to the problem (11) with the boundary condition (17) and the initial condition:

$$T(z,t=0)=0 \tag{18}$$

is derived in Appendix for the case where $V_s(t)$ and $\tau(t)$ are constants. Since $V_s(t)$ and $\tau(t)$ vary over the time and are temperature dependent, following Kato (2001), we subdivide the time interval [0,t] in a discrete number N of sub-intervals where $V_s(t), \tau(t)$ and T(t) can be assumed to be constants. In this way the expression (a19), given in Appendix, becomes:

$$T(0,t)=T_{ini}+$$
$$+\sum_{i=1}^{N}\frac{V_s(t_{i-1})\tau(t_{i-1})\eta_{sf}}{2K_{sf}}\left\{\begin{array}{l}\left[\left(\frac{1}{U}+\frac{U(t-t_i)}{2\eta_{sf}}\right)erf\left(\frac{U}{2}\sqrt{\frac{(t-t_i)}{\eta_{sf}}}\right)-\frac{U(t-t_i)}{2\eta_{sf}}+\sqrt{\frac{(t-t_i)}{\pi\eta_{sf}}}\exp\left(-\frac{U^2(t-t_i)}{4\eta_{sf}}\right)\right]+\\ -\left[\left(\frac{1}{U}+\frac{U(t-t_{i-1})}{2\eta_{sf}}\right)erf\left(\frac{U}{2}\sqrt{\frac{(t-t_{i-1})}{\eta_{sf}}}\right)-\frac{U(t-t_{i-1})}{2\eta_{sf}}+\sqrt{\frac{(t-t_{i-1})}{\pi\eta_{sf}}}\exp\left(-\frac{U^2(t-t_{i-1})}{4\eta_{sf}}\right)\right]\end{array}\right\} \tag{19}$$

where:

$$U=\frac{(\rho_w C_w)}{(\rho C)_{sf}}v \tag{20}$$

In equation (19) t_0=0, t_N=t and $T_{ini}=T(z=0,t=0)$ is the background temperature **and erf(x) denotes the value assumed in x by the error function.** Using the same approach, from equation (a20) of the Appendix we obtain the time derivative of the temperature in z=0:

$$\left(\frac{\partial T}{\partial t}\right)_{z=0}=-\sum_{i=1}^{N}\frac{V_s(t_{i-1})\tau(t_{i-1})}{2K_{sf}}\left\{\begin{array}{l}\left[-\frac{U}{2}erfc\left(\frac{U}{2}\sqrt{\frac{(t-t_i)}{\eta_{sf}}}\right)+\sqrt{\frac{\eta}{\pi t_i}}\exp\left(-\frac{U^2(t-t_i)}{4\eta_{sf}}\right)\right]+\\ \left[\frac{U}{2}erfc\left(\frac{U}{2}\sqrt{\frac{(t-t_{i-1})}{\eta_{sf}}}\right)-\sqrt{\frac{\eta}{\pi t_{i-1}}}\exp\left(-\frac{U^2(t-t_{i-1})}{4\eta_{sf}}\right)\right]\end{array}\right\} \tag{21}$$

In equation (21) erfc(x) denotes the value assumed in x by the complementary error function. The proposed formulation allows us to consider only the evolution of temperature along the fault plane (z=0). For this reason the partial derivative with respect to time in equation (21) $\left(\frac{\partial T}{\partial t}\right)_{z=0}$ **coincides with the total time derivative** $\left(\frac{dT}{dt}\right)$ **to be used in equation (7).**

The equations (6), (7) and (21) represent a system of coupled first order differential equations in the unknowns V_s, τ and T to be solved simultaneously.

2.4 THE TEMPERATURE EVOLUTION IN THE CASE OF A TIME DEPENDENT FLUID VELOCITY

In the previous paragraph we derived an expression of the temperature field for the case of a constant velocity perpendicular to the fault plane. In the frame of the fluid migration model described in section 2.2, this could happen only in the case of a negligible thermal pressurization effect. In this section we describe how we account for the thermal pressurization effect in our model. If pore pressure varies as a consequence of the temperature variations along the fault (equation 10), the fluid velocity will also vary. In particular, from the equations (8) and (9) and (10) it follows that:

$$\left.\frac{\partial v(t)}{\partial t}\right|_{z=0} = -\frac{H}{\gamma\phi}\frac{\partial}{\partial t}\frac{\partial p}{\partial z} = -\left.\frac{H\Gamma}{\gamma\phi}\frac{\partial^2 T(t)}{\partial t \partial z}\right|_{z=0} \qquad (22)$$

where z is the coordinate on an axis perpendicular to the fault plane (fig. 1). As an effect of the pore fluid pressure variations, the effective normal stress on the fault plane will also vary over the time:

$$\sigma_n^{eff} = \sigma_n - p(t) \qquad (23)$$

From equation (10) it follows that:

$$\frac{d}{dt}\sigma_n^{eff} \approx -\Gamma\left.\frac{dT}{dt}\right|_{z=0} \qquad (24)$$

To include the velocity variations of fluids, we use the same approach described in the previous section, i.e. we subdivide the time interval $0 \le t \le T_{\max}$ in N sub-intervals where the fluid velocity is a constant:

$$\begin{aligned} &v_i = v(t) \qquad t_{i-1} \le t < t_i \qquad 1 \le i \le N \\ &t_0 = 0 \\ &t_N = T_{\max} \end{aligned} \qquad (25)$$

As a consequence, in the time interval $0 \le t \le T_{\max}$, the energy equation (11) is subdivided into N equations:

$$\eta_{sf}\frac{\partial^2 T}{\partial z^2} - \frac{(\rho_w C_w)}{(\rho C)_{sf}} v_i \frac{\partial T}{\partial z} = \frac{\partial T}{\partial t} \quad 1 \le i \le N \qquad (26)$$

These equations have to be solved with the same previously described conditions (equations (17) and (18)) and the continuity of the temperature at each t_i. Following the same lines described in the previous paragraph, it can be easily shown that the solution to this problem is simply obtained by

substituting v with v_{i-1} in equation (19). The same substitution has to be made in the expression of the time derivative of the temperature (equation (21)).

Therefore, the mechanical evolution of the system is, in this case, inferred by solving the system of five first order differential equations given by (6), (7), (21), (22) and (24).

3. RESULTS

In what follows we show the results of the numerical simulations carried out using the two models described in section 2 and compare the results with those arising from the use of the purely conductive energy equation (Kato 2001).

The solutions of the systems of first order differential equations have been obtained using a MATLAB® script to incorporate an explicit Runge Kutta method (ode45 in MATLAB® documentation) with an adaptative time-step size control to ensure the accuracy of solutions. Some of the parameters used in the simulations have been fixed, once and for all, to the values summarized in Table 1.

In the simulations we have to assume a constant value of the permeability H. For this reason, in what follows, we generally show the simulation results as a function of H. H is known to vary greatly with rock type and thermodynamical state; a great range of variations ($10^{-20} < H < 10^{-8}$ m^2) has been inferred for different types of rocks in different conditions (e.g. Turcotte and Schubert 1982). Moreover, near a fault, local variations in permeability have been often inferred. For example, Jourde *et al*. (2002) studied the permeability of the faults in the Valley of Fire State Park, Nevada. They estimated that the permeability of several fault zones can suffer strong lateral variations depending also on the focal mechanism. Jourde *et al*. (2002) reported that the presence of joints can give rise to a strong local increase of permeability (until to 10^{-9} m^2). The same order of magnitude for permeability has been proposed by Jahr *et al*. (2005) to model the fluid transport around a fault zone near the KTB borehole (> 1 km of depth). In their study on earthquake instability, Lockner and Byerlee (1995) assumed a permeability of the order of $6 \cdot 10^{-12}$ m^2. Moreover, Wibberley and Shimamoto (2003) provided evidence that permeability can strongly increase in the direction normal to the fault plane. This result has been supported further by the simulation results of Bizzarri and Cocco (2006A). The local variations in hydraulic properties of the faults have been well summarized by the experiments led by Cappa *et al*. (2005) which show that fluid flow in the fault zone is controlled by dual-permeability behavior, with highly permeable subfaults (H=10^{-12} m^2) bounding low-permeable rock-matrix blocks (H=10^{-18} m^2). In the simulation results of Cappa *et al*. (2007), the permeability of the rocks near a fault ranges from a minimum

H=10^{-19} m^2 for the fault core to an intermediate H=10^{-12} m^2 for the inherited planes to a maximum of H=10^{-8} m^2 for the fault-related fractures.

3.1 SIMULATION RESULTS FOR THE CONSTANT SLIP VELOCITY AND THE CONSTANT SHEAR STRESS

First of all we have analyzed the temperature rise vs. time on the fault plane, considering, for sake of simplicity, a constant slip velocity (V_s=10^{-5} m s^{-1}) and a constant shear stress on the fault $\sigma_n^{eff} = 200$ MPa. Fig.2 shows the temperature on the fault plane for different values of permeability, as given by equation (a19). As expected, the temperature disturbance due to the frictional heating decreases with increasing the rock permeability (and then the fluid velocity). This is because a higher permeability allows heat to be easily transferred far from the fault and therefore only smaller increments of temperature on the fault plane are allowed.

In fig. 2 we have assumed a constant value of the thermal conductivity of the solid phase (K_s=2.6 W m^{-1} K^{-1}), as derived from laboratory measurement on crustal rocks (Kato 2001).

In the next simulation (fig. 3) we have evaluated the effect on temperature of small variations of thermal parameters around their typical values. It is in fact well known that the thermal parameters are dependent on the pressure, the temperature and the fluid content of the rocks (e.g. Chapman and Furlong 1991). Therefore a more rigorous approach to the energy equation should take into account the dependence of K_s on the depth z, the temperature T and the fluid content of the rocks. However, since $K_s(z,T)$ strongly depends also on the rock type (Beardsmore and Cull 2001), the functional form of $K_s(z,T)$ for a given rock type could not be the same for another rock type. Moreover the dependence of K_s on z and T gives rise to a non linearity of the energy equation and only numerical method can be used to approximately solve this problem. Therefore we have tried to evaluate how much the results can be affected by reasonable variations in the thermal parameters. For this reason, in fig. 3, we consider how the thermal disturbance on the fault plane varies if we vary K_s of ±10%, for a fixed value of rock permeability (H=10^{-13} m^2). As an effect of varying K_s also the thermal conductivity of solid phase η_s will vary (equations 12 and 13). We note that an increase in K_s and η_s results in a temperature reduction on the fault plane, as it could be obtained by increasing the permeability of the system (fig.2). This implies that H is correlated with the thermal parameters η_s and K_s on the temperature vs. time curves.

3.2 SIMULATION RESULTS FOR THE TIME VARYING SLIP VELOCITY AND SHEAR STRESS: THE CONSTANT FLUID VELOCITY CASE

Let us consider now the most general case where slip, stress and temperature vary together. **In agreement with recent studies (Belardinelli *et al.* 2003; Rubin and Ampuero 2005; Antonioli *et al.* 2006) we assume V=0.1 m s^{-1}as the limit value for the occurrence of instability.**

First, we consider the simulation results for the case of a constant fluid velocity. Even if this model is only an approximation of the most general case where fluid velocity is allowed to vary as a consequence of the thermal pressurization effect, it allows us to understand the key role played by the average permeability of the rocks surrounding the fault. Therefore these simulations refer to real cases of fault planes surrounded by rocks characterized by a small coefficient of pressurization (Γ < 0.01 MPa K^{-1}) (Mase and Smith 1987).

In these simulations, the model parameters are chosen so that the simulation might express pre-seismic sliding of a large earthquake on the San Andreas fault, California and are summarized in table I. Friction parameters a, b, the effective normal stress σ_n^{eff} and the initial temperature T_{ini} are approximately the same as those assumed for the nucleation site of a large earthquake on the San Andreas fault in the simulation study by Kato (2001).

In our simulations, fluid velocity has been derived using equations (8) and (9) under the assumption of a pressure regime where $|\nabla p| = \rho_w g$, being ρ_w the density of the fluids and g the gravity acceleration.

By neglecting the thermal effect on the friction coefficient (unheated case) the critical stiffness, i.e. the stiffness which separates the stable from the unstable regime, in the velocity weakening regime (a-b<0) is given by (Rice and Ruina 1983; Ruina 1983):

$$k_c^0 = \frac{(b-a)\sigma_n^{eff}}{L} \qquad (27)$$

Fig.4 shows the entire temporal evolution of the pre-seismic phase for the case H= 10^{-14} m^2, whereas Fig. 5 shows a zoom on the final evolution of the pre-seismic phase, parameterized as a function of H. In fig.4 and fig. 5 we assumed $\sigma_n^{eff} = 200$ MPa, $k = k_c^0 = 10^8$ Pa m^{-1}, a background temperature T_{ini}= 550 K and the other model parameters summarized in table 1. Independently on permeability, with this choice of the model parameters, an unstable sliding phase occurs. The main effect of including the heat advection effect consists of a time delay of the onset of instability t_s with respect to the purely conductive case. This time delay ranges from about 1.8 hours for H=10^{-15} m^2 to about 3.8 hours for H=10^{-14} m^2; it has un upper limit equal to about 4 hours for the unheated case, namely the case where the temperature effects are neglected in the friction laws. In our simulations, for H ≥ 10^{-10} m^2 all curves conform to the unheated curves. In contrast, for small permeability values (H ≤ 10^{-20} m^2) all curves conform to that of the purely conductive case (Kato 2001). Another result consists in the different values attained by the temperature rise on the fault plane, which

progressively decrease with increasing H (from a maximum of about 175 K after t=1800 s for the case H=10^{-20} m^2 until to a nil value for H>10^{-10} m^2).

Fig. 6 shows the simulation results using the same model parameters of Fig. 4 (Table I), $\sigma_n^{eff} = 200$ MPa and $k = 5k_c^0 = 5 \cdot 10^8$ Pa m^{-1}. Fig.7 shows the simulation results, parameterized as a function of H, using the model parameters of Table I and $k = 5 \cdot 10^8$ Pa m^{-1}. In these cases, the system is always subjected to the stable sliding regime, independently on the value of permeability. As for the unstable case, the time at which the maximum of slip velocity is attained increases with increasing the permeability of the fault, even if the differences are smaller. Also in this case, for H< 10^{-20} m^2, the curves conform with that of the purely conductive case, whereas, for H≥10^{-10} m^2, the curves conform with that of the unheated case (Fig. 7). The peak of slip velocity slightly decreases with increasing permeability and the same occurs for the maximum value attained by the slip. As expected, the peak of temperature tends to decrease with increasing H.

3.3 SIMULATION RESULTS FOR THE CASE OF A TIME VARYING SLIP VELOCITY AND SHEAR STRESS: THE THERMAL PRESSURIZATION REGIME

Let us consider now the simulation results obtained by using the model which accounts for the pore pressure variation due to temperature, described in section 2.4. Results of simulations are summarized in Fig. 8 and Fig. 9. In figure 8 the curves for $\sigma_n^{eff}(t=0) = 200$ MPa, k=10^8 Pa/m, H=10^{-21} m^2 and two different values of Γ (0.1 and 1.1 MPa K^{-1}) are reported, together with the curves of the purely conductive case (Kato 2001). The simulation results have a physical significance quite different from that inferred for the case of a constant fluid velocity. In fact, as an effect of the thermal pressurization effect, a time advance of the onset of instability t_s, with respect to the model of Kato (2001), is now inferred. The reason for this trend is that, as an effect of the increase of pore pressure, the effective normal stress on the fault plane decreases faster than in the purely conductive case, allowing the slip velocity to increase faster. Fig. 8 clearly indicates that this time advance is proportional to the values of the thermal pressurization factor Γ. In fact it increases from about 0.9 hours for the case Γ=0.11 MPa K^{-1} to about 10.2 hours for the case Γ=1.1 MPa K^{-1}. Moreover, whereas in the initial stage of the pre-seismic phase, fluid velocity, pore pressure and the temperature on the fault slowly increase, they suffer a more pronounced increase near to the onset of instability.

Another point we investigated was represented by the values assumed by the critical stiffness of the transition between stable and unstable sliding. Kato (2001) noted that the critical stiffness k_c, which is inversely dependent on the critical length of the nucleation zone, is shifted toward higher values in the purely conductive case. Since the seismic moment M_0 of the preseismic phase is proportional

to the cube fault length and therefore is inversely dependent on the stiffness of the system, Kato (2001) concluded that M_0 is smaller than in the unheated case. We have made new calculations, using the two models described in the sections 2.3 and 2.4, to compute the critical stiffness for different values of the ratio V_0/V_{ini}. Using the model which does not include the effect of thermal pressurization (section 2.3), with H=10^{-15} m^2, σ_n^{eff} =200 MPa and T_{ini}=550 K, we found out that k_c is the same as that found by Kato (2001). On the contrary, when the effect of thermal pressurization is taken into account (section 2.4) the results are significantly different. We made the simulations assuming Γ=1.1 MPA K^{-1}, H=10^{-20} m^2, σ_n^{eff} =200 MPa and T_{ini}=550 K (Fig.9). We found that k_c tends to be systematically higher than that obtained by Kato (2001). This results indicate that, on a heated fault and in the thermal pressurization regime, unstable sliding may occur with a stiffer system. In particular, the ratio between the critical stiffness in the thermal pressurization regime and the critical stiffness in the purely conductive case ranges from a minimum of 1.13 to a maximum of 1.21.

Ellsworth and Beroza (1995, 1998) identified a nucleation phase of slow moment release and suggested that the duration of this feature could scale with the eventual size of the earthquake. Even if this argument is controversial, owing to the difficulty in distinguishing the source from the path effect in the early stage of the first P pulses (see e.g. de Lorenzo et al. 2008 and references therein), under these assumptions an attempt can be made to estimate the seismic moment of the pre-seismic phase. Since the critical length l_c of the nucleation zone scales with L, according to the equation (Bizzarri and Cocco 2003):

$$l_c = \frac{\eta G L}{(b-a)\sigma_n^{eff}},$$

η being a geometrical, dimensionless, numerical parameter and G the rigidity of rocks surrounding the fault surface, we have:

$$M_0^{ps} \propto l_c^3 \propto k_c^{-3}$$

It follows that M_0^{ps} in the thermal pressurized regime is from 30 to 44 per cent smaller than in the purely conductive regime and that l_c in the thermal pressurized regime is from 12 to 18 per cent smaller than in the purely conductive regime.

4. CONCLUSION

An analytical solution to the energy equation which includes the heat advection effect has been derived, for the case of a constant shear stress and a constant slip velocity on the fault plane. Using the approach proposed by Kato (2001), this solution has been generalized to the case of time

varying shear stress and slip velocity on the fault and therefore can be used to describe the pre-seismic sliding phase in the frame of the rate-, state- and temperature-dependent friction laws, for both the case of a constant fluid velocity model and the case of fluid velocity variations caused by thermally induced pore pressure variations.

Simulation results show important differences from the purely conductive case described by Kato (2001). **The first conclusion that can be drawn from the present study is that, in the case of a constant fluid velocity, the time differences in the occurrence of the unstable sliding phase, with respect to the Kato (2001) model, are very small. For example, for the case described in fig. 4 and 5, these differences are in the order of about 0.1- 0.2 days (relative variations in the order of 0.02%).**

The **second** conclusion is that the evolution of the pre-seismic sliding phase is primarily controlled by the values of the thermal pressurization factor Γ and the permeability H of the rocks surrounding the fault plane. For small values of Γ the description of the evolution of the pre-seismic sliding phase can be simplified by considering the constant fluid velocity model described in section 2.3. In this case, the main effect of heat advection is a delay of the onset of instability of the system with respect to the purely conductive case; it increases with increasing rock permeability. For higher values of Γ ((Γ >.01 MPa K^{-1}) the behavior of the pre-seismic phase is the opposite, with the onset of instability always preceding the onset of instability of the purely conductive case. In particular, in this Γ–range the trend of curves is strongly dependent on permeability. For $H<10^{-18}$ m^2, pore pressure monotonically increases and the velocity weakening regime is maintained until the instability is reached. Finally, for typical values of permeability of ultracataclastic gouge ($H<10^{-19}$ m^2) (Rice 2006), the thermal pressurization effect may result in significantly smaller values of the seismic moment and nucleation length of the pre-seismic phase. Following Kato (2001), this could imply a smaller crustal deformation before an earthquake.

A further effort has to be made to evaluate the effect of some assumptions made in this study. First of all, an aspect that has to be considered in future studies is the effect of allowing the state variable θ to vary over the time. Moreover, some aspects in the thermal evolution along the fault, such as the changes of state (Stefan 1891), the chemical reactions occurring during faulting (due, for instance, to water absorption) and the mechanical lubrication (Brodsky and Kanamori 2001) have been neglected. This is because it is not possible, in these cases, to infer a pseudo-analytical temperature solution to be used in the frame of a first order system of differential equations and only numerical methods in 2D media can help us to solve all these problems.

Aknowledgments. We are grateful to Naoyuchi Kato for giving us its code for the calculation of the preseismic slip for the heated case and for many explanations of the content of his paper. We thank Stefan Nielsen for his reading of an early manuscript. **A comment of Giorgio Ranalli on the model assumptions allowed us to better define the significance of the model. Giorgio Ranalli and an anonymous reviewer are acknowledged for their valuable comments which significantly improved the article.** This research has been supported by University of Bari funds.

REFERENCES

Abramowitz, M., Stegun, I. A., 1965. Handbook of Mathematical Functions, Dover Publications, Inc., New York, USA

Andrews, D.J., 2005. Rupture dynamics with energy loss outside the slip zone, J. Geophys. Res. 110, B01307, doi: 10.1029/2004JB003191.

Antonioli, A., Piccinini, D., Chiaraluce, L., Cocco, M., 2005. Fluid flow and seismicity pattern: Evidence from the 1997 Umbria- Marche (central Italy) seismic sequence, Geophys. Res. Lett. 32, L10311, doi:10.1029/2004GL022256.

Antonioli, A., Belardinelli, M. E., Bizzarri, A., Vogfjord, K. S., 2006. Evidence of instantaneous dynamic triggering during the seismic sequence of year 2000 in south Iceland, J. Geophys. Res. 111, B03302, doi:10.1029/2005JB003935.

Beardsmore, G.R., Cull, J.P., 2001, Crustal Heat Flow, A Guide to Measurement and Modeling, Cambridge University Press, Cambridge, USA.

Beeler, N.M., Tullis, T. E., Kronenberg, A. K., Reinen, L. A., 2007. The instantaneous rate dependence in low temperature laboratory rock friction and rock deformation experiments, J. Geophys. Res. 112, B07310, doi: 10.1029/2005JB003772.

Belardinelli, M.E., Bizzarri, A., Cocco, M., 2003. Earthquake triggering by static and dynamic stress changes, J. Geophys. Res. 108, NO. B3, 2135, doi:10.1029/2002JB001779.

Bizzarri, A., Cocco, M., 2003. Slip-weakening behavior during the propagation of dynamic ruptures obeying rate- and state-dependent friction laws, J.Geophys. Res. 108, B8, 2373, doi:10.1029/2002JB002198.

Bizzarri, A., Cocco M., 2006A. A thermal pressurization model for the spontaneous dynamic rupture propagation on a three-dimensional fault: 1. Methodological approach, J. Geophys. Res. 111, B05303, doi:10.1029/2005JB003862.

Bizzarri, A., Cocco, M., 2006B. A thermal pressurization model for the spontaneous dynamic rupture propagation on a three-dimensional fault:2. Traction evolution and dynamic parameters, J. Geophys. Res. 111, B05304, doi: 10.1029/2005JB003864.

Blanpied, M. L., Lockner, D. A., Byerlee, J. D.,1995. Frictional slip of granite at hydrothermal conditions, J. Geophys. Res. 100, B7, 13.045-13,064.

Blanpied, M.L., Tullis, T.E., Weeks, J.D., 1998. Effects of slip, slip rate, and shear heating on the friction of granite, J. Geophys. Res. 103, 489–511.

Brodsky, E. E., Kanamori, H., 2001. Elastohydrodynamic lubrication on faults, J. Geoph. Res.., 106, B8, 16,357-16,375

Caggianelli, A., de Lorenzo, S., Prosser, G., 2005. Modelling the heat pulses generated on a fault plane during coseismic slip: Inferences from the pseudotachylites of the Copanello cliffs (Calabria, Italy), Tectonophysics 405, 99– 119.

Cappa, F., Guglielmi, Y., Fe´nart, P., Merrien, V. and Thoraval, A., 2005. Hydromechanical interactions in a fractured carbonate reservoir inferred from hydraulic and mechanical measurements, Int. J. Rock Mech. Min. Sci. 42, 287– 306.

Cappa F., Guglielmi, Y., Virieux, J., 2007. Stress and fluid transfer in a fault zone due to overpressures in the seismogenic crust, Geophys. Res. Lett. 34, L05301, doi: 10.1029/2006GL028980.

Cardwell, R. K., Chinn, D. S., Moore, G. F., Turcotte, D. L., 1978. Frictional heating on a fault zone with finite thickness, Geophys .J. R. Astron. Soc. 52, 525– 530.

Carslaw, H.S., Jaeger, J.C., 1959. Conduction of Heat in Solids, (2nd edition), Oxford University Press, New York, USA.

Chapman, D. S., Furlong, K. P., 1991. Thermal state of the continental crust, in Continental Lower Crust, pp. 179–199, Elsevier, New York.

Chester, F.M., 1994. Effect of temperature on friction: constitutive equations and experiments with quartz gouge, J. Geophys. Res. 99, B4, 7247-7261

Chester, F.M., 1995. A rheologic model for wet crust applied to strike-slip faults, J. Geophys. Res. 100, B7, 13,033-13,044.

Chester, F.M. , Higgs, N.G., 1992. Multimechanism friction constitutive model for ultrafine quartz gouge at hydrothermal conditions, J. Geophys. Res. 97, 1859–1870.

Chester, F. M., and Chester, J.S., 1998. Ultracataclasite structure and friction processes of the Punchbowl fault, San Andreas system, California, Tectonophysics, 295,199-221.

Cocco, M., Bizzarri, A., 2002. On the slip-weakening behavior of rate- and state dependent constitutive laws, Geophys. Res. Lett. 29, NO. 11, 1516, 10.1029/2001GL013999

de Lorenzo, S., Filippucci, M., Boschi, E., 2008. An EGF technique to infer the rupture velocity history of a small magnitude earthquake J. Geophys. Res.,113, B10314, doi:10.1029/2007JB005496, 2008

Di Toro, G., Hirose, T., Nielsen, S., Pennacchioni G., Shimamoto, T., 2006. Natural and experimental evidence of melt lubrication of faults during earthquakes, Science 311, 647-649.

Dieterich, J.H., 1979. Modeling of rock friction, 1, Experimental results and constitutive equations, J. Geophys. Res. 84, 2161–2168.

Dieterich, J.H., 1992. Earthquake nucleation on faults with rate- and state-dependent strength, Tectonophysics 211, 115-134.

Ellsworth, W. L., Beroza, G. C., 1995. Seismic evidence for a seismic nucleation phase, Science, 268, 851-855.

Ellsworth, W. L., Beroza, G. C., 1998. Observation of the seismic nucleation phase in the Ridgecrest, California, earthquake sequence, Geophys. Res. Lett., 25(2), 401–404.

Fialko, Y., 2004. Temperature fields generated by the elastodynamic propagation of shear cracks in the Earth, J. Geophys. Res. 109, B01303, doi:10.1029/2003JB002497.

Goyal, K. P., Narasimhan, T. N., 1982. Heat and Mass Transfer in a Fault-Controlled Geothermal Reservoir Charged at Constant Pressure, J. Geophys. Res., 87(B10), 8581–8590.

Guéguen, Y., Dormieux, B., Boutéca M, 1997, Fundamentals of Poromechanics in Mechanics of Fluid-Saturated Rocks (eds. Y. Guéguen and M. Boutéca), pp. 1-54, International Geophysics Series, Elsevier Academic Press vol. 89.

Hirose, T., Shimamoto, T., 2005. Growth of molten zone as a mechanism of slip weakening of simulated faults in gabbro during frictional melting, J. Geophys. Res. 110, B05202, doi:10.1029/2004JB003207.

Incropera, F. P., DeWitt, D. P., 1996, Fundamentals of heat and Mass Transfer, John Wiley and sons, 4th Edition, New York, USA.

Jahr, T., Jentzsch, G., Letz, H. and Sauter, M., 2005. Fluid injection and surface deformation at the KTB location: modelling of expected tilt effects, Geofluids 5, 20–27.

Jourde, H., Flodin, E. A., Aydin, A., Durlofsky, L. J., Wen, X.H., 2002. Computing permeability of fault zones in eolian sandstone from outcrop measurements, AAPG Bull. 86, 1187–1200.

Kato, N., 2001. Effect of frictional heating on pre-seismic sliding: a numerical simulation using a rate-, state- and temperature-dependent friction law, Geophys. J. Int. 147, 183–188

Lachenbruch, A. H., 1980. Frictional heating, fluid pressure and the resistance to fault motion, J. Geophys. Res., 85, 6097–6112.

Lockner, D. A., Byerlee, J.D., 1995. An earthquake instability model based on faults containing high-fluid pressure compartments. Pageoph, 145, 717-743.

Lorenzetti, E., Tullis, T. E., 1989. Geodetic predictions of a strike-slip fault model: Implications for intermediate- and short-term earthquake prediction, J. Geophys. Res. 94(B9), 12343-12361, 10.1029/89JB00663.

Madariaga, R., 2007. Slippery When Hot, Science 316 (5826), 842 – 843 doi: 10.1126/science.1142332.

Mair, K., and C. J. Marone, Friction of simulated fault gauge for a wide range of velocities and normal stresses, J. Geophys. Res., 104, 28,889–28,914, 1999

Mase, C. W., Smith, L., 1987, Effects of frictional heating on the thermal, hydrologic, and mechanical response of a fault, J. Geophys. Res. 92, 6249–6272.

McKenzie, D., Brune, J. N., 1972. Melting on fault planes during large earthquakes, Geophys. J. R. Astr. Soc. 29, 65–78.

Miller, S. A., Collettini, C., Chiaraluce, L., Cocco, M., Barchi, M., Boris, J., Kraus P., 2004. Aftershocks driven by a high-pressure CO2 source at depth, Nature 427, 724– 727.

Noir, J., Jacques, E., Bekri, S., Adler, P. M., Tapponier, P., King G. C. P., 1997. Fluid flow triggered migration of events in the 1989 Dobi earthquake sequence of central Afar, Geophys. Res. Lett. 24, 2335– 2338.

Rice, J. R., 2006. Heating and weakening of faults during earthquake slip, J. Geophys. Res. 111, B05311, doi:10.1029/2005JB004006.

Rice, J. R., Ruina, A. L., 1983. Stability of steady frictional slipping, J. Appl. Mech. 50, 343–349.

Rubin, A. M., Ampuero, J.-P. 2005, Earthquake nucleation on (aging) rate and state faults, J. Geophys. Res. 110, B11312, doi:10.1029/2005JB003686.

Ruina, A.L., 1983. Slip instability and state variable friction laws, J. Geophys. Res. 88, 10 359–10 370.

Scholz, C. H. 1990. The mechanics of earthquakes and faulting, Cambridge University Press, Cambridge, USA

Scholz, C. H. 1998. Earthquakes and friction laws, Nature, 39, 37-42

Scholz, C. H. 2002. Evidence for a strong San Andreas fault, Geology 28 (2); 163-166; doi: 10.1130/0091-7613.

Segall, P., Rice, J. R., 2006. Does shear heating of pore fluid contribute to earthquake nucleation?, J. Geophys. Res., 111, B09316, doi:10.1029/2005JB004129

Sibson, R. H., 1973. Interaction between temperature and pore-fluid pressure during earthquake faulting—A mechanism for partial or total stress relief, Nature 243, 66–68.

Sibson, R. H., 2003. Thickness of the seismic slip zone, Bull. Seism. Soc. Am., 93, 1169-1178

Stefan, J., 1891. Über die Theorie der Eisbildung, insbesondere über Eisbildung im Polarmeere. Ann. Phys. 42, 269–286.

Svesnichov, A. G., and Tichonov, A. N. 1984, Teoria delle funzioni di variabili complesse,Editori Riuniti, Roma, Edizioni Mir, Mosca.

Turcotte, D. L., Schubert, G., 1982. Geodynamics, John Wiley and Sons, New York, USA.

Wibberley, C. A. J., Shimamoto, T., 2003. Internal structure and permeability of major strike-slip fault zones: The Median Tectonic Line in mid prefecture, southwest Japan, J. Struct. Geol. 25, 59–78.

Williams, C. F., Narasimhan, T.,N., 1989. Hydrogeologic constraints on heat flow along the San Andreas fault: a testing of hypotheses, Earth Plan. Sci. Lett. 92,131-143

APPENDIX

We consider the Laplace transform $\Psi(z)$ of the temperature $T(z,t)$:

$$\Psi(p,z)=\int_0^\infty e^{-pt}T dt \quad p>0 \tag{a1}$$

By applying the Laplace transform to the equation (11) it follows that (see Carslaw and Jaeger, 1959 for details):

$$\eta_{sf}\frac{d^2\Psi}{dz}-U\frac{d\Psi}{dz}-p\Psi=0 \tag{a2}$$

where:

$$U=\frac{(\rho_w C_w)}{(\rho C)_{sf}}v \tag{a3}$$

The boundary conditions (17) transforms into:

$$\left[-K_{sf}\Psi'+\frac{K_{sf}}{\eta_{sf}}U\Psi\right]_{z=0}=\frac{1}{p}\frac{V_s\cdot\tau}{2} \tag{a4}$$

The solution to equation (a2) which does not diverge when $z\to\infty$ is given by:

$$\Psi=C\exp\left[\left(\frac{U}{2\eta_{sf}}-\sqrt{\left(\frac{U}{2\eta_{sf}}\right)^2+\frac{p}{\eta_{sf}}}\right)z\right] \tag{a5}$$

By substituting (a5) in (a4) the value of the integration constant C is found to be:

$$C=\frac{V_s\tau}{2pK\left(\frac{U}{2\eta_{sf}}+\sqrt{\left(\frac{U}{2\eta_{sf}}\right)^2+\frac{p}{\eta_{sf}}}\right)} \tag{a6}$$

and therefore, substituting (a6) in (a4) it follows that:

$$\Psi=\frac{V_s\tau}{2pK_{sf}\left(\frac{U}{2\eta_{sf}}+\sqrt{\frac{1}{\eta_{sf}}\left(p+\frac{U^2}{4\eta_{sf}}\right)}\right)}\exp\left[\left(\frac{U}{2\eta_{sf}}-\sqrt{\frac{1}{\eta_{sf}}\left(p+\frac{U^2}{4\eta_{sf}}\right)}\right)z\right] \tag{a7}$$

The temperature can be found by computing the inverse transform of (a7):

$$T(z,t)=\Psi^{-1}\Psi(p) \tag{a8}$$

By posing:

$$p'=p+\frac{U^2}{4\eta_{sf}} \tag{a9}$$

It follows (Carslaw and Jaeger, 1959):

$$T(z,t) = \exp(-\frac{U^2 t}{4\eta_{sf}})\Psi^{-1}\Psi(p') \tag{a10}$$

where $\Psi^{-1}\Psi(p')$ has to be computed using the Inversion theorem of the Laplace transform (Carslaw and Jaeger, 1959):

$$\Psi^{-1}\Psi(\lambda) = \frac{1}{2\pi i}\frac{V_s \tau \exp\left(\frac{Uz}{2\eta_{sf}}\right)}{2K_{sf}} \int_{\gamma-i\infty}^{\gamma+i\infty} \frac{e^{\lambda t - \sqrt{\frac{\lambda}{\eta_{sf}}}z}}{\left(\lambda - \frac{U^2}{4\eta_{sf}}\right)\left(\frac{U}{2\eta_{sf}} + \sqrt{\frac{\lambda}{\eta_{sf}}}\right)} d\lambda \tag{a11}$$

The evaluation of the integral in (a11) is performed by using the Cauchy theorem of residuals (e.g. Svesnichov and Tichonov, 1984):

$$\frac{1}{2\pi i}\oint_{\Gamma} f(\lambda)d\lambda = \sum_{i=1}^{N} res\left(f(\lambda), \lambda_i\right) \tag{a12}$$

where $f(\lambda)$ is an analytical function of the complex variable λ in all the points of the complex plane with the exception of N points $\lambda_1,..,\lambda_N$ where f has removable singularities. The closed oriented contour Γ has to be chosen to include all the singularities of f and to leave the domain which includes the singularities at its left. The integrand in equation (a11) has only a first order singularity (a pole) on the real plane:

$$\lambda_1 = \frac{U^2}{4\eta_{sf}} \tag{a13}$$

and the residual of f in $\lambda = \lambda_1$ is given by:

$$res\left[f, \lambda = \lambda_1\right] = \frac{e^{\frac{U^2 t}{4\eta_{sf}} - \sqrt{\frac{U^2}{4\eta_{sf}^2}}z}}{\frac{U}{2\eta_{sf}} + \sqrt{\frac{U^2}{4\eta_{sf}^2}}} = \frac{\eta_{sf}}{U} e^{\frac{U}{2\eta_{sf}}\left(\frac{Ut}{2} - z\right)} \tag{a14}$$

Since f has a branch point in $\lambda_b = 0$, following Carslaw and Jaeger (1959), we used the closed integration contour Γ reported in fig. (a1). By letting tend the radius R of the great circle to infinity and the radius ρ of the small circle to zero the contribution to the integral comes only from the oriented branches AB, FE and DC.

By posing $\lambda = \rho e^{i\pi}$ along the branch FE and $\lambda = \rho e^{-i\pi}$ along the branch DC, after some manipulations it follows that the contribution of these two branches to the integral in (a12) is given by:

$$\int_0^\infty \frac{e^{-\rho t - iz\sqrt{\frac{\rho}{\eta_{sf}}}}}{\left(-\rho - \frac{U^2}{4\eta_{sf}}\right)\left(\frac{U}{2\eta_{sf}} + i\sqrt{\frac{\rho}{\eta_{sf}}}\right)} d\rho - \int_0^\infty \frac{e^{-\rho t + iz\sqrt{\frac{\rho}{\eta_{sf}}}}}{\left(-\rho - \frac{U^2}{4\eta_{sf}}\right)\left(\frac{U}{2\eta_{sf}} - i\sqrt{\frac{\rho}{\eta_{sf}}}\right)} d\rho \qquad \text{(a15)}$$

Therefore, by taking into account (a14), equation (a11) furnishes:

$$\Psi^{-1}\Psi(p') = \frac{V_s \tau \exp\left(\frac{Uz}{2\eta_{sf}}\right)}{2K_{sf}} \left\{ \frac{\eta_{sf}}{U} e^{\frac{U}{2\eta_{sf}}\left(\frac{Ut}{2} - z\right)} - \frac{1}{2\pi i} \int_0^\infty e^{-\rho t} \frac{e^{-iz\sqrt{\frac{\rho}{\eta}}}\left(\frac{U}{2\eta_{sf}} - i\sqrt{\frac{\rho}{\eta_{sf}}}\right) - e^{iz\sqrt{\frac{\rho}{\eta_{sf}}}}\left(\frac{U}{2\eta_{sf}} + i\sqrt{\frac{\rho}{\eta_{sf}}}\right)}{\left(-\rho - \frac{U^2}{4\eta_{sf}}\right)\left(\frac{U^2}{4\eta_{sf}^2} + \frac{\rho}{\eta_{sf}}\right)} d\rho \right\} \qquad \text{(a16)}$$

By substituting (a16) in (a10), after a few manipulations, it follows that:

$$T(z,t) = \frac{V_s \tau \eta_{sf}}{2K_{sf}} \left\{ \frac{1}{U} - \frac{\exp\left(\frac{Uz}{2\eta_{sf}} - \frac{U^2 t}{4\eta_{sf}}\right)}{\pi} \int_0^\infty e^{-\rho t} \frac{\sqrt{\frac{\rho}{\eta_{sf}}} \cos z\sqrt{\frac{\rho}{\eta_{sf}}} + \frac{U}{2\eta_{sf}} \sin z\sqrt{\frac{\rho}{\eta_{sf}}}}{\left(\frac{U^2}{4\eta_{sf}} + \rho\right)^2} d\rho \right\} \qquad \text{(a17)}$$

In z=0 the previous expression gives:

$$T(0,t) = \frac{V_s \tau \eta_{sf}}{2K_{sf}} \left\{ \frac{1}{U} - \frac{\exp\left(-\frac{U^2 t}{4\eta_{sf}}\right)}{\pi\sqrt{\eta_{sf}}} \int_0^\infty e^{-\rho t} \frac{\sqrt{\rho}}{\left(\frac{U^2}{4\eta_{sf}} + \rho\right)^2} d\rho \right\} \qquad \text{(a18)}$$

Integrating by parts, the integral in (a18) reduces to classical tabulated integrals (Abramowitz and Stegun, 1965). The solution is:

$$T(0,t) = \frac{V_s \tau \eta_{sf}}{2K_{sf}} \left\{ \left(\frac{1}{U} + \frac{Ut}{2\eta_{sf}}\right) erf\left(\frac{U}{2}\sqrt{\frac{t}{\eta_{sf}}}\right) - \frac{Ut}{2\eta_{sf}} + \sqrt{\frac{t}{\pi\eta_{sf}}} \exp\left(-\frac{U^2 t}{4\eta_{sf}}\right) \right\} \qquad \text{(a19)}$$

where erf(x) denotes the value in x of the error function.

It can be easily verified that, by letting *v* tend to zero (i.e. no fluid transport), the temperature solution (a19) tends to the solution inferred from McKenzie and Brune (1972) for the purely conductive case.

By carrying out spatial and time derivatives of the temperature field it can be shown that:

$$\frac{\partial T(0,t)}{\partial t} = \frac{V_s \tau}{2K_{sf}} \left\{ -\frac{U}{2} erfc\left(\frac{U}{2}\sqrt{\frac{t}{\eta_{sf}}}\right) + \sqrt{\frac{\eta_{sf}}{\pi t}} \exp\left(-\frac{U^2 t}{4\eta_{sf}}\right) \right\} \qquad \text{(a20)}$$

and:

$$\left(\frac{\partial^2 T}{\partial t \partial z}\right)_{z=0} = -\frac{V_s \tau U}{2K_{sf}}\left[\frac{U}{2\eta_{sf}} erfc\left(\frac{U}{2}\sqrt{\frac{t}{\eta_{sf}}}\right) - \sqrt{\frac{1}{\pi \eta_{sf} t}} \exp\left(-\frac{U^2 t}{4\eta_{sf}}\right)\right] \quad \text{(a21)}$$

where erfc(x) denotes the value in x of the complementary error function.

Table 1. Parameter values assumed in the simulations

μ_0= 0.6
a = 0.012
b = 0.017
L=10^{-2} m
Q_a =10^5 J mol^{-1}
Q_b = 10^5 J mol^{-1}
ρ_s=2.6·10^3 kg m^{-3}
ρ_w=10^3 kg m^{-3}
C_s=1000 J kg^{-1} K^{-1}
C_w=4186 J kg^{-1} K^{-1}
K_s=2.6 W m^{-1}K^{-1}
K_w=0.603 W m^{-1}K^{-1}
ϕ=0.1
η= 10^{-6} m^2 s^{-1}
V_0= 3.5 cm yr^{-1}
γ=1.14· 10^{-3} Pa s

Figure Caption

Fig.1- a) representation of the symmetrical flux lines of fluids in the fault core. b) The spring block model and the reference system used to solve the heat advection problem. The surface between the rigid block and the floor simulates the fault plane. u_0 is the load-point displacement and u is the displacement of the rigid block. v is the average value of the fluid velocity in the fault core

Fig.2 Temperature vs. time curves for a constant slip rate and a constant shear stress (see the text). The different curves refer to different values of permeability given in the legend.

Fig. 3 Temperature vs. time curves for a constant slip rate and a constant shear stress (see the text). The different curves are obtained considering a ten percent of variations of thermal parameters.

Fig. 4 Simulated slip, slip rate, shear stress and temperature histories for the cases $k/k_c^0 = 1$ and H=10^{-14} m^2 using the model with a constant fluid velocity. The entire evolution of the system is shown.

Fig. 5 Simulated slip, slip rate, shear stress and temperature histories for the cases $k/k_c^0 = 1$ using the model with a constant fluid velocity, for different values of permeability. The evolution of the system around the onset of instability is shown. **For $H \geq 10^{-8}$ m^2 the curves superimpose on curve 1, whereas for $H \leq 10^{-21}$ m^2 the curves superimpose on curve 4**.

Fig. 6 Simulated slip, slip rate, stress and temperature histories for the case $k/k_c^0 = 5$ and H=10^{-14} m^2 using the model with a constant fluid velocity. The entire evolution of the system is shown.

Fig. 7 Simulated slip, slip rate, stress and temperature histories for the case $k/k_c^0 = 5$ m^2 using the model with a constant fluid velocity, for different values of permeability. The evolution of the system around the peak value of slip velocity is shown.

Fig. 8 Simulated slip, slip rate, shear stress, fluid velocity, pore pressure and temperature histories for the cases $k/k_c^0 = 1$ using the model with a time varying fluid velocity, for two different values of the thermal pressurization coefficient Γ. The evolution of the system around the onset of instability is shown.

Fig. 9 Plot of the critical stiffness vs. V_0/V_{ini}

Fig. a1. The close contour Γ used to compute the integral (a12)

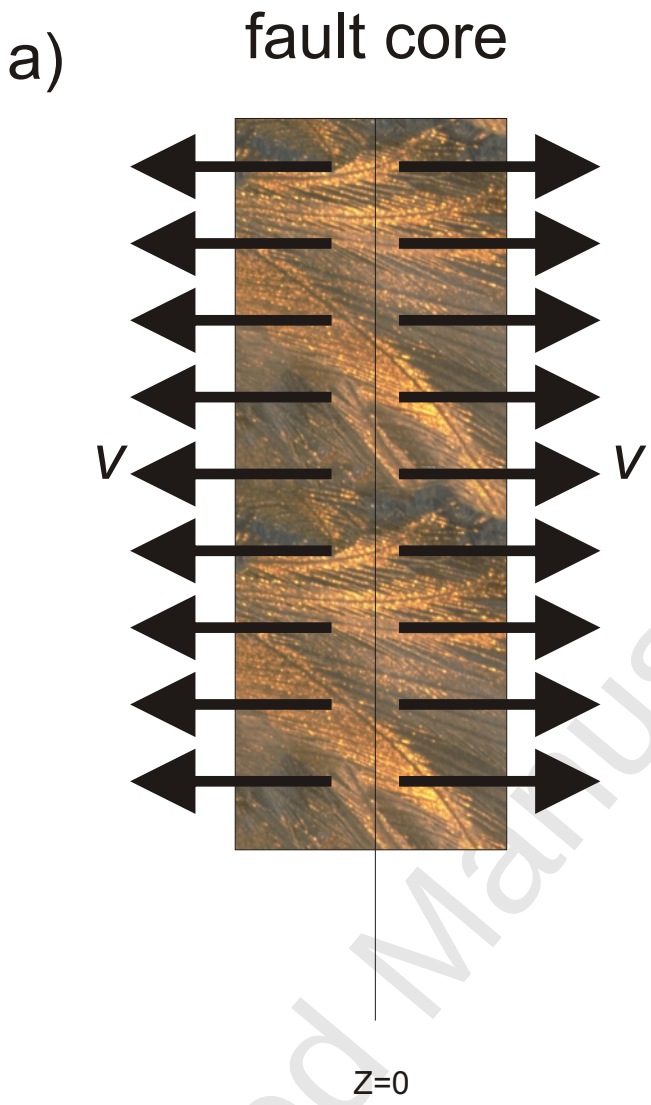

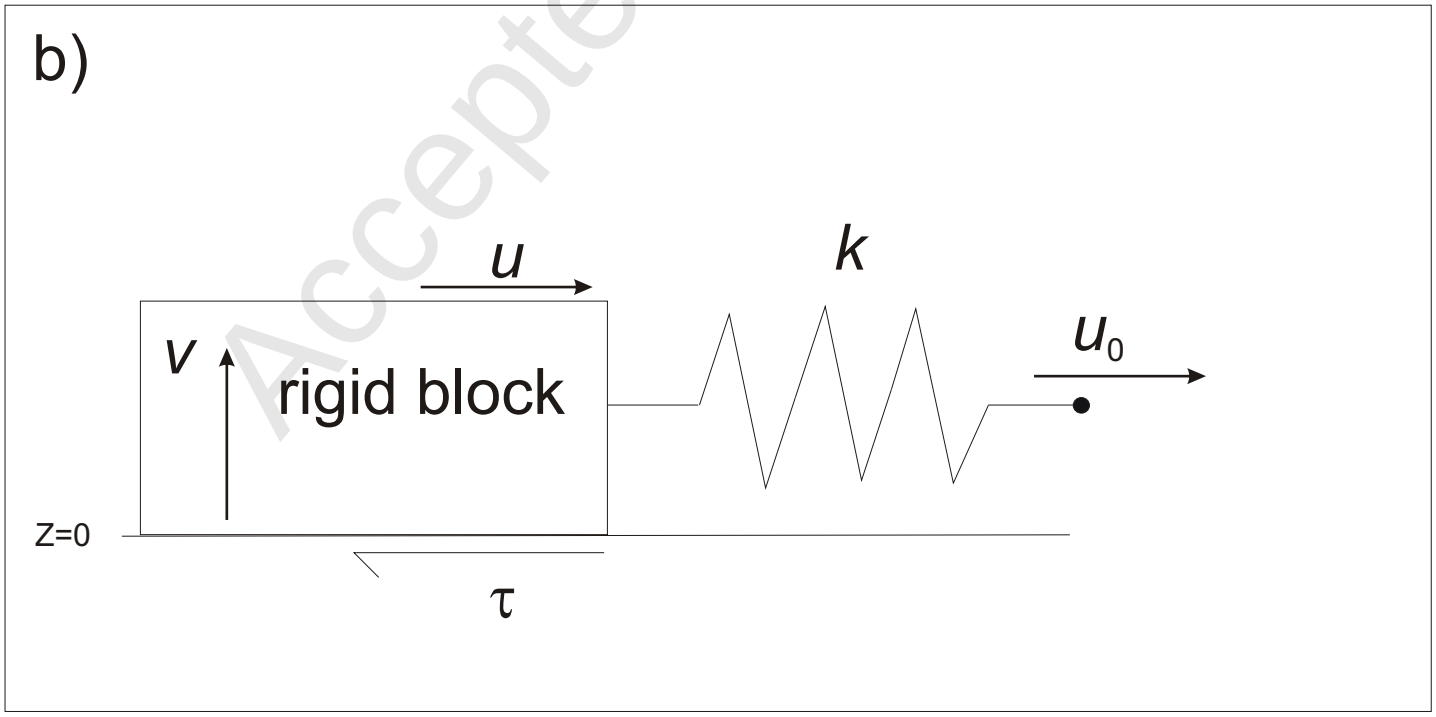

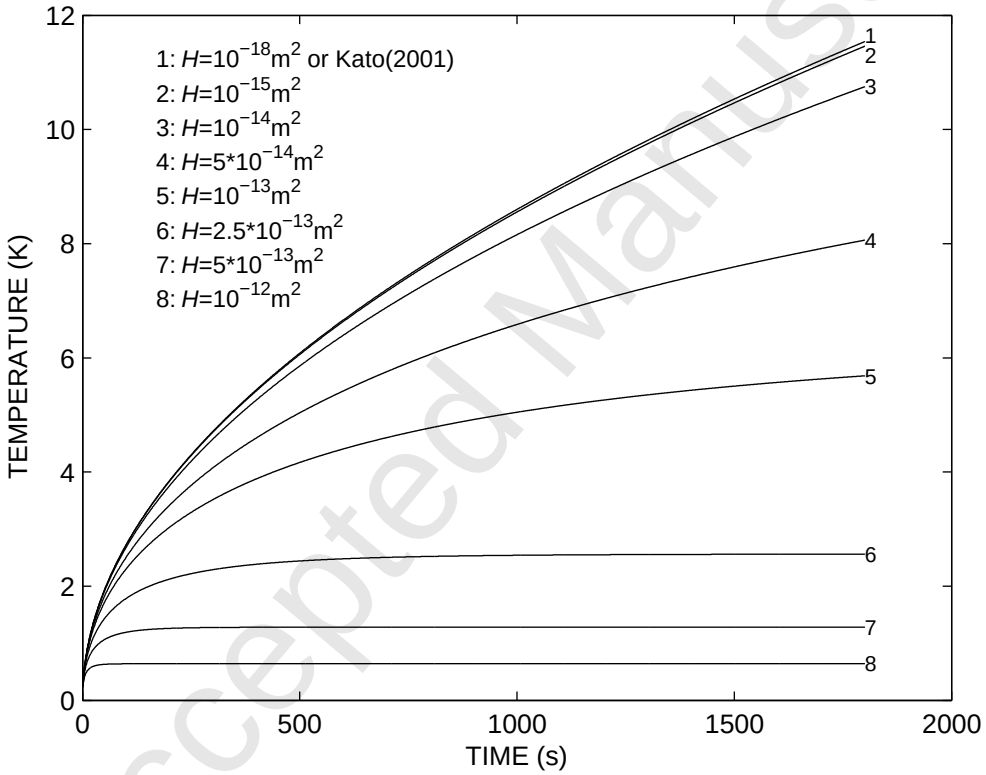

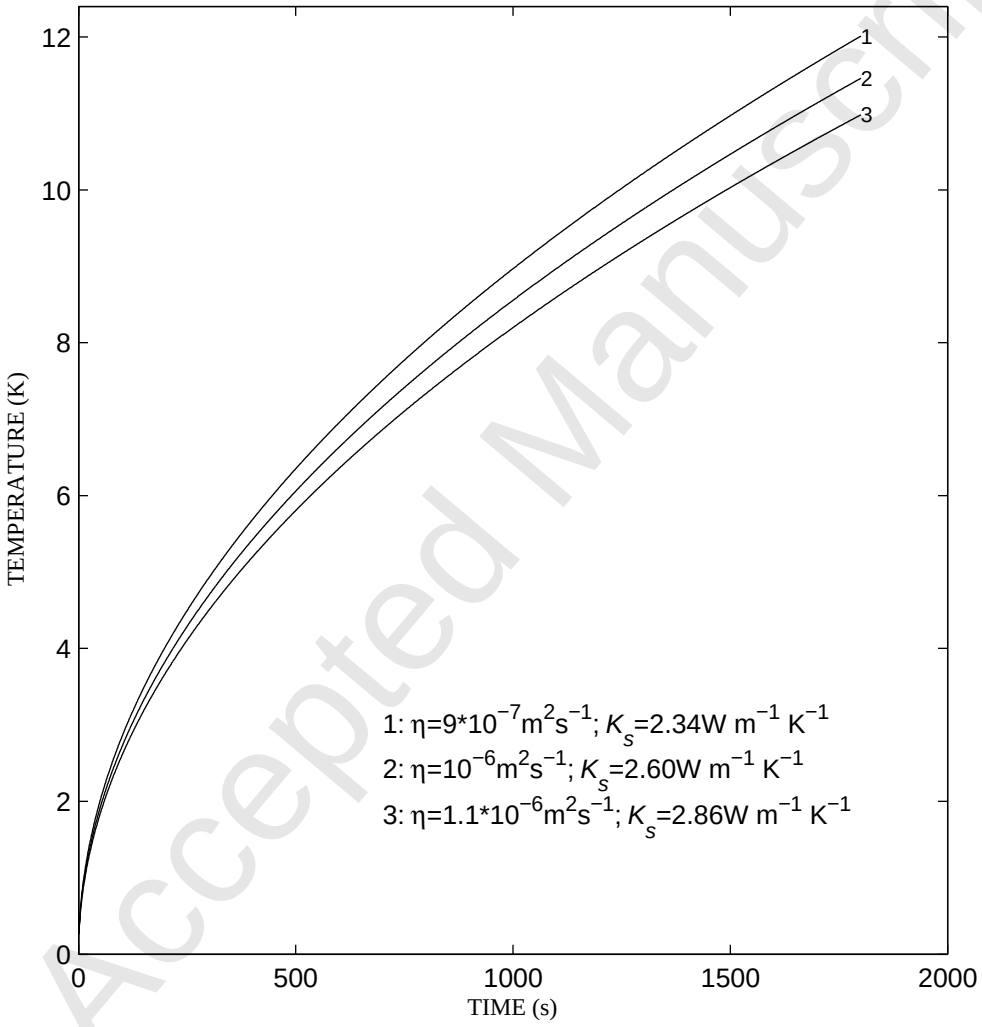

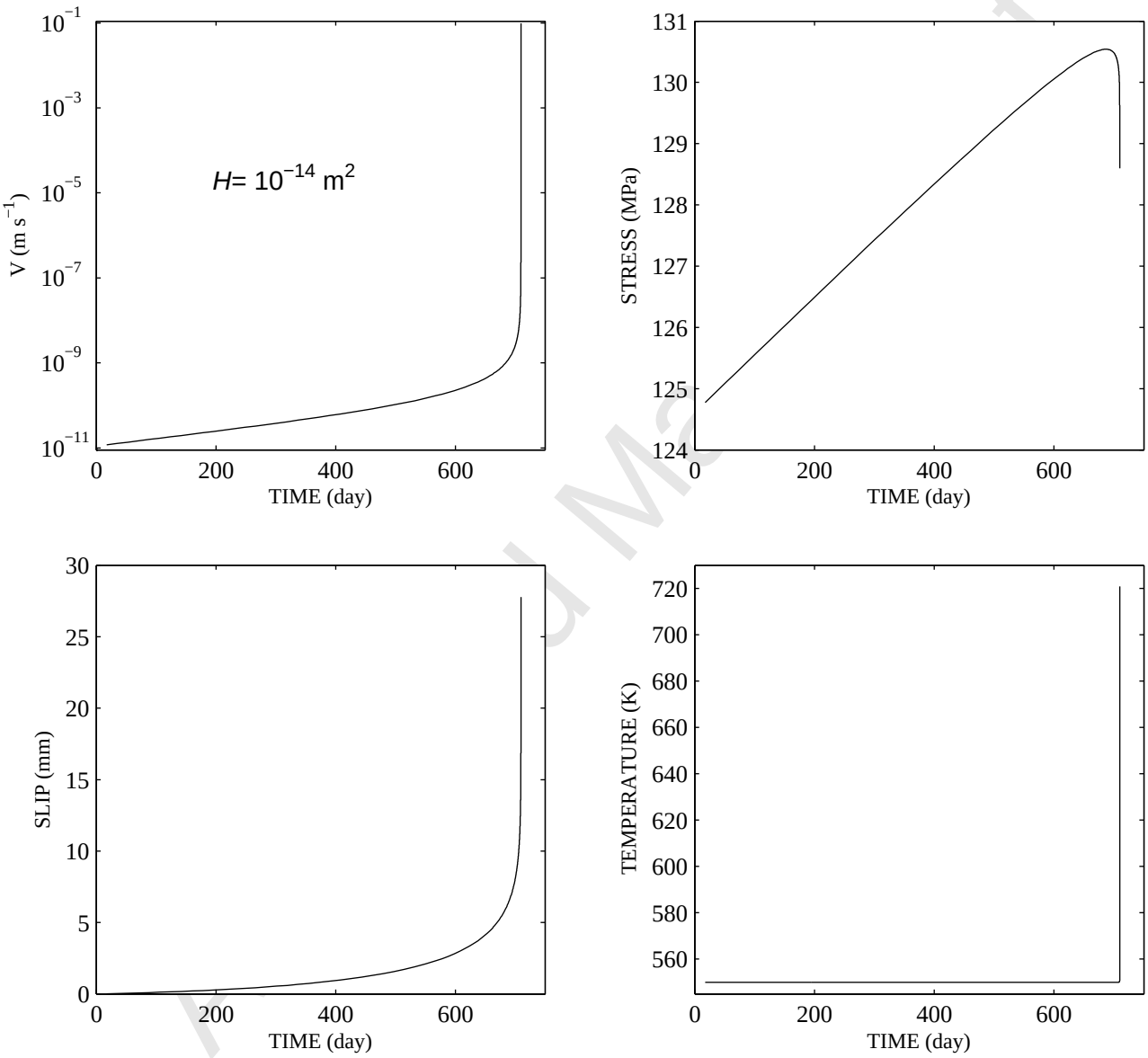

figure 4

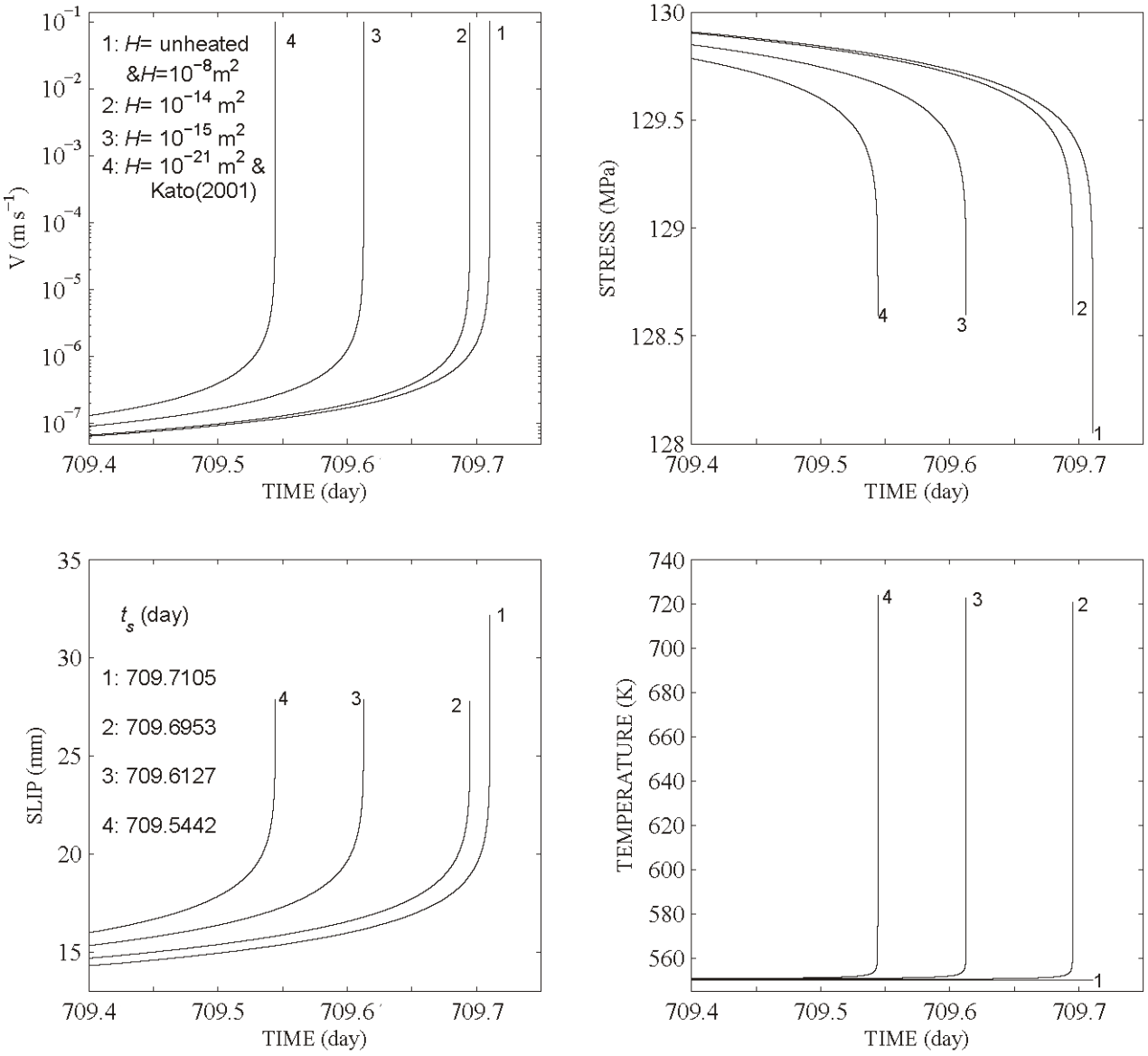

figure 5

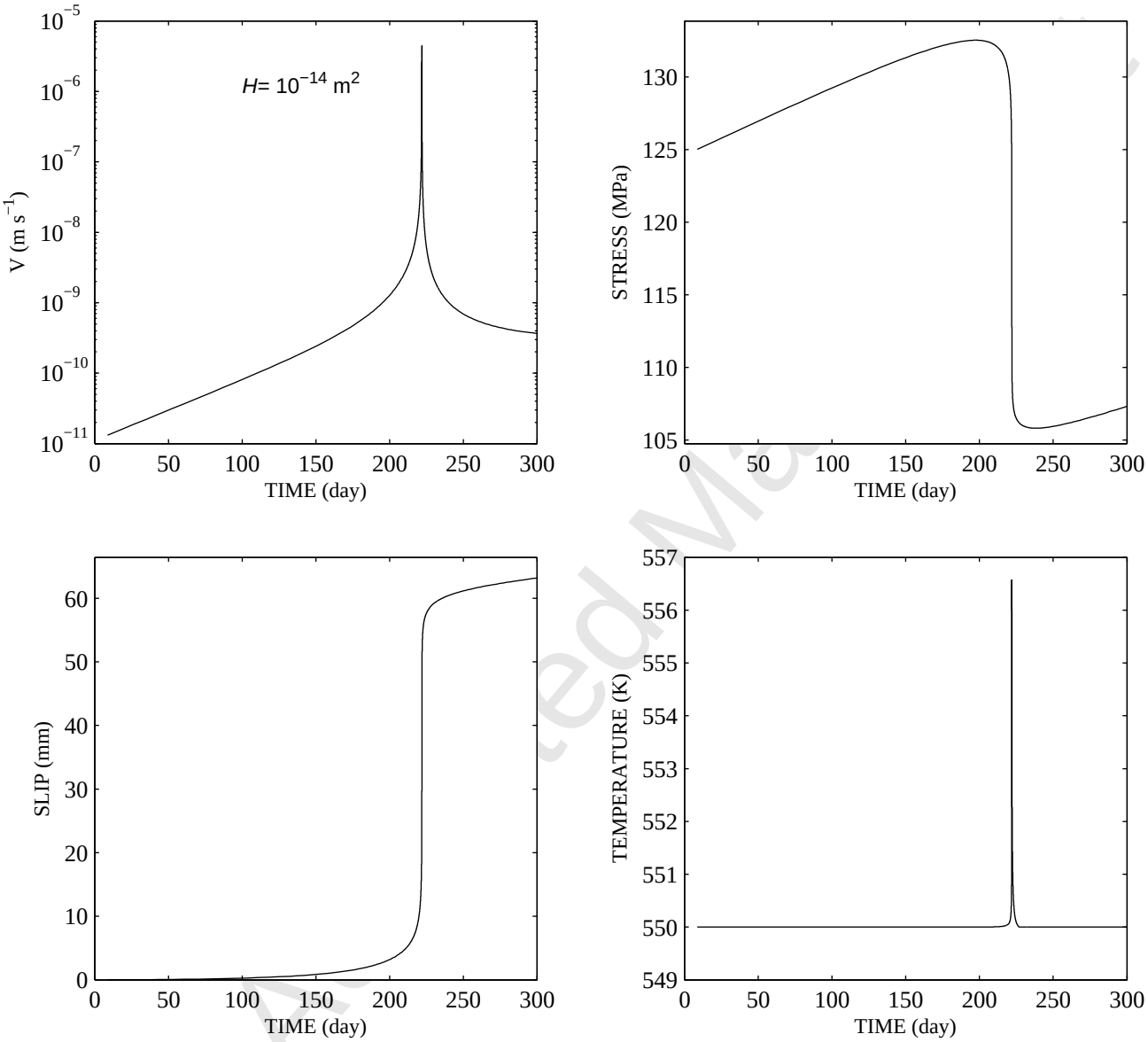

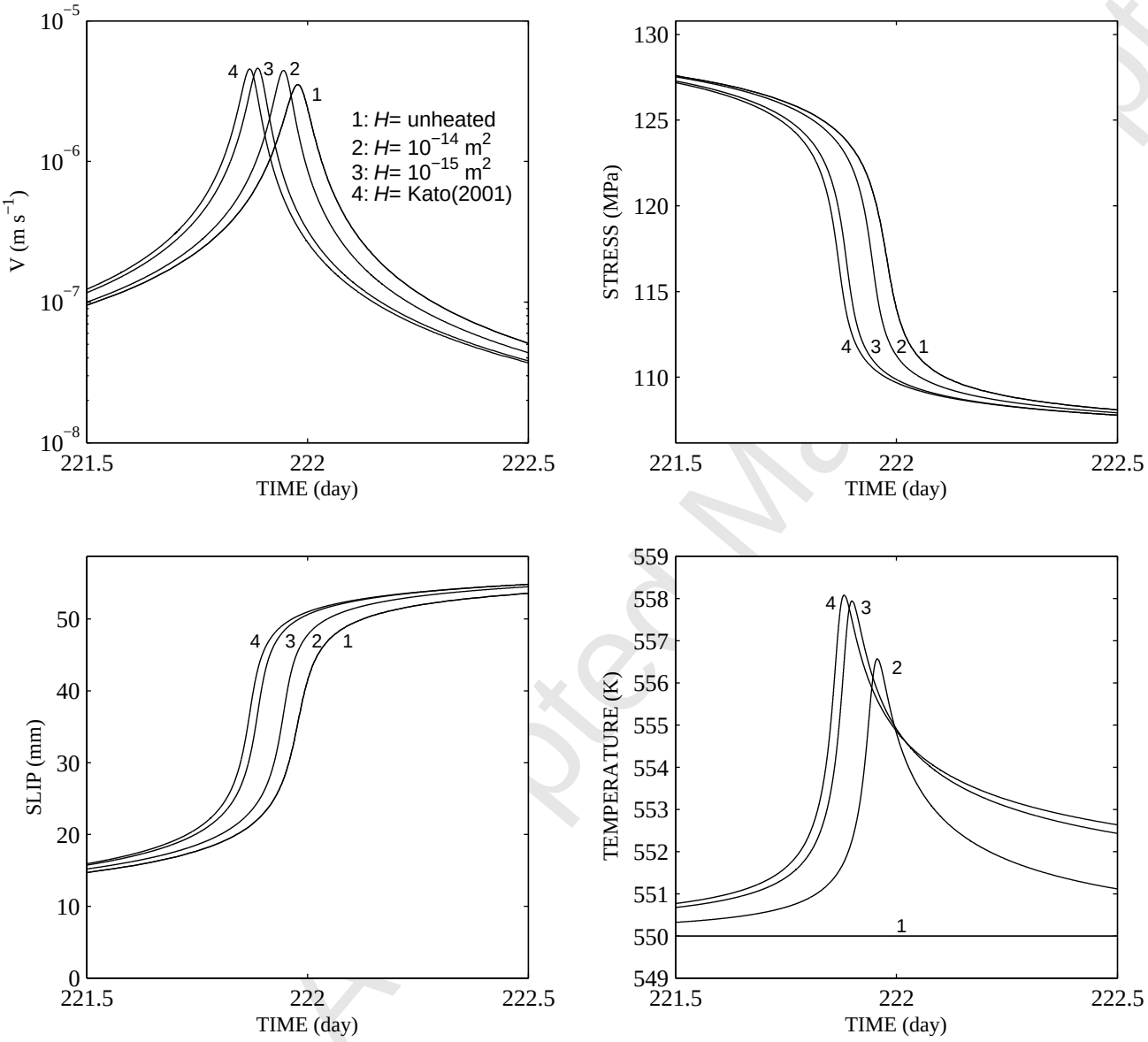

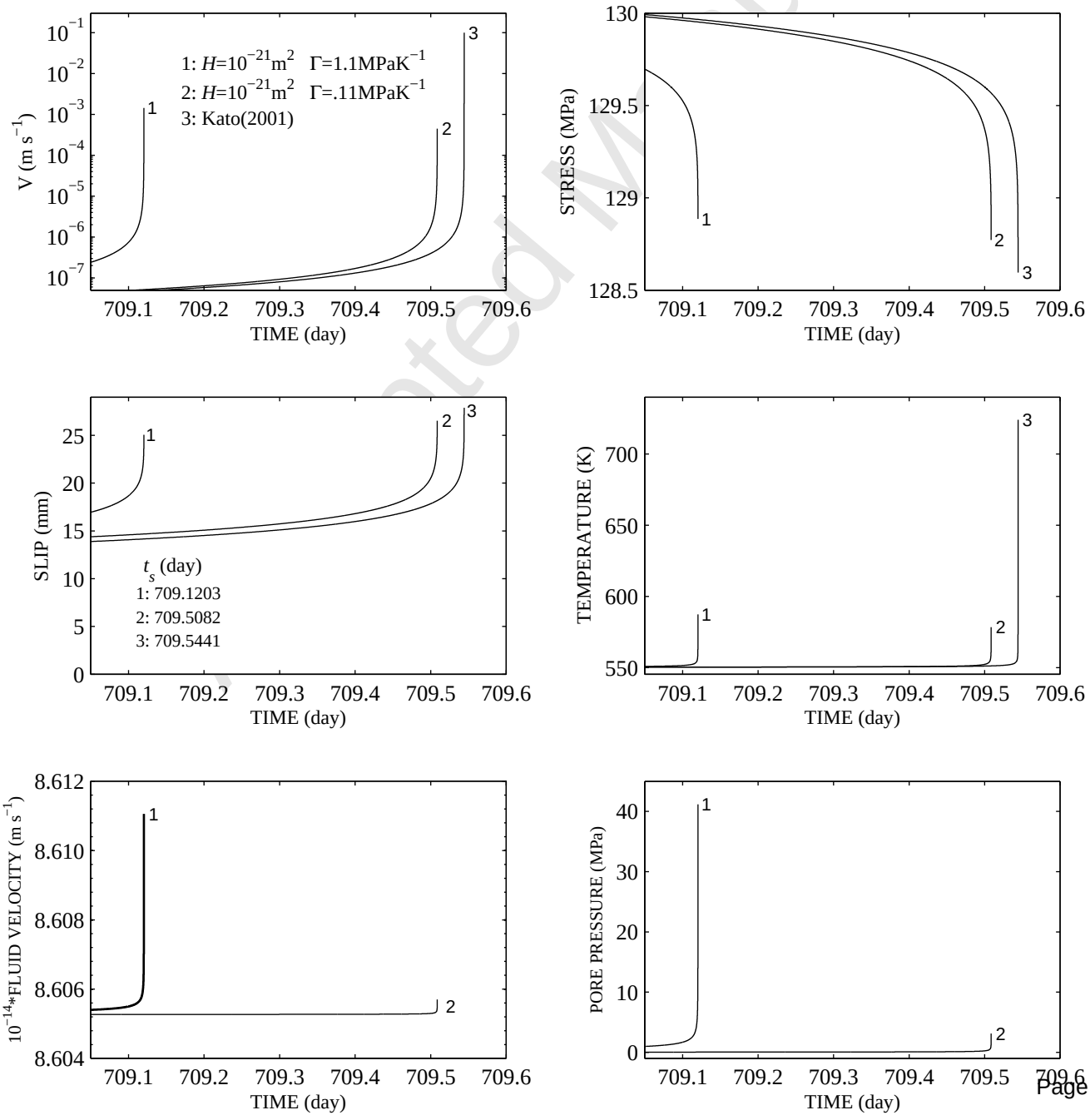

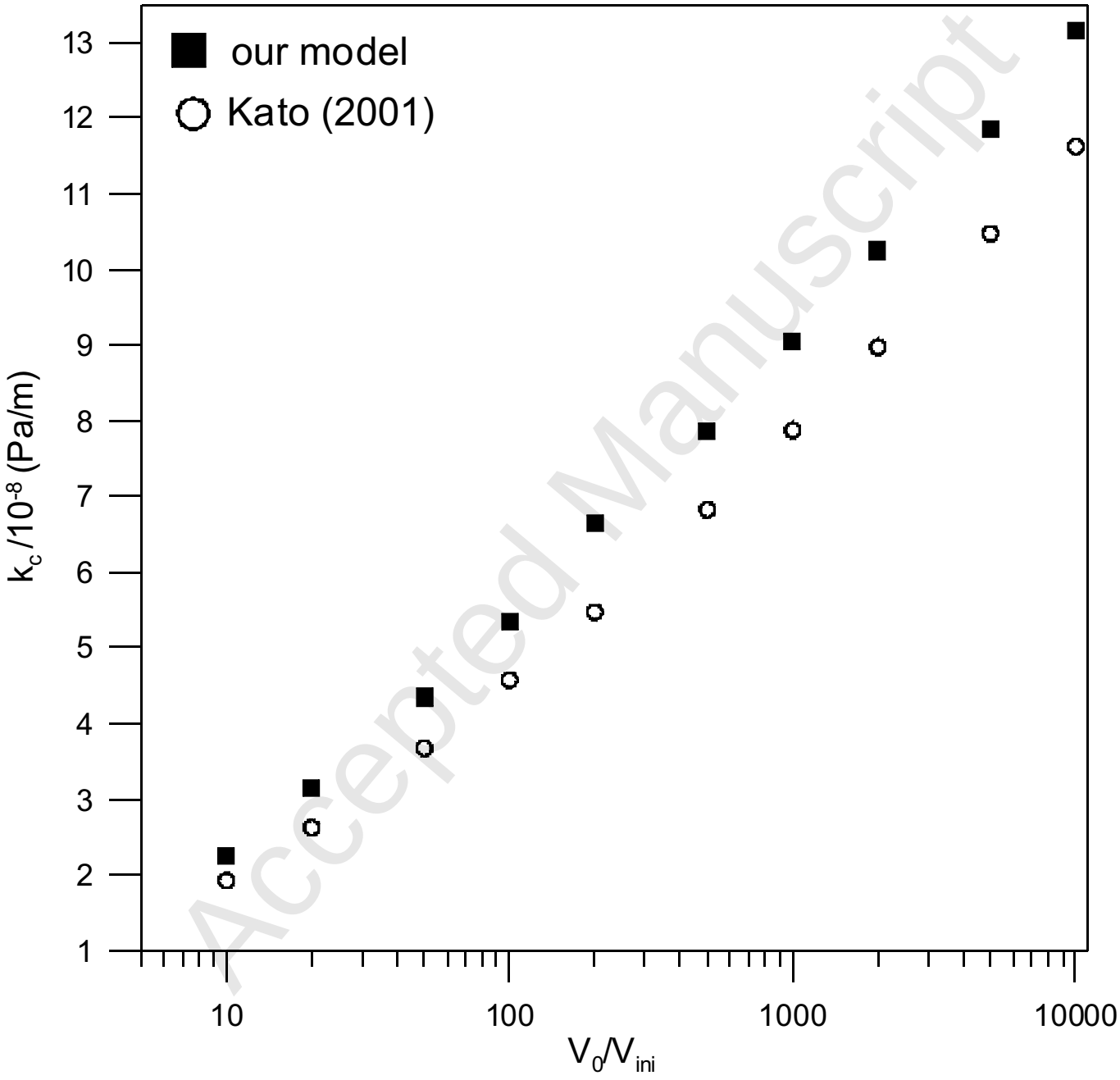

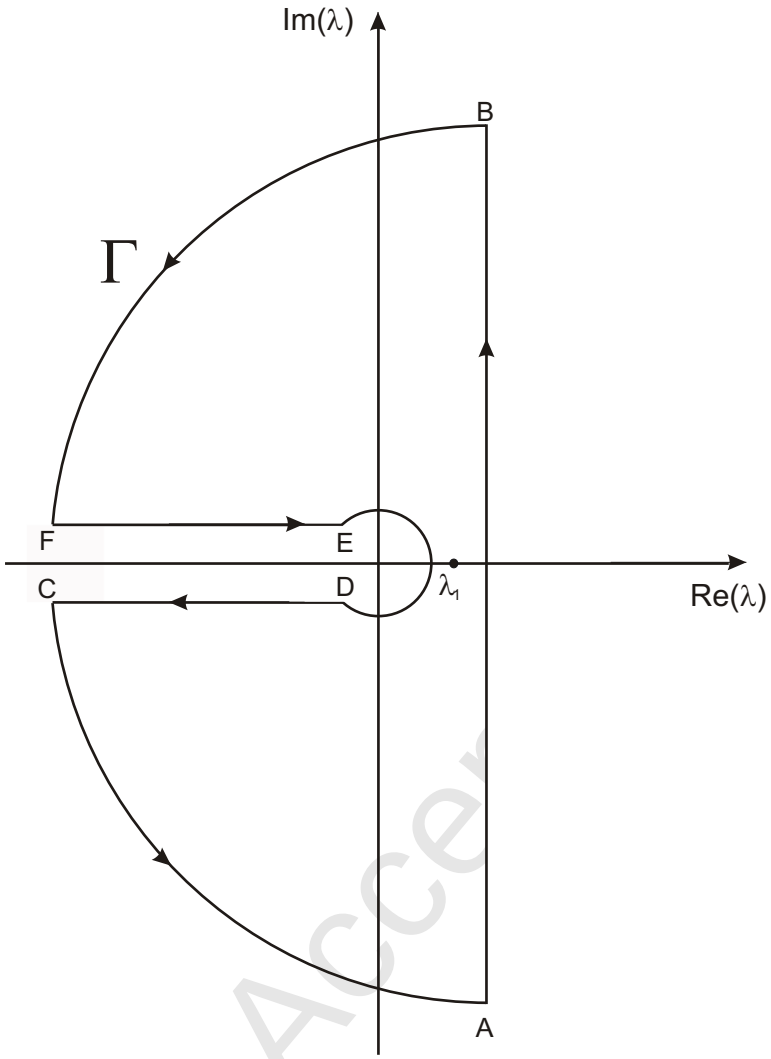

Table 1. Parameter values assumed in the simulations

μ_0= 0.6
a = 0.012
b = 0.017
L=10^{-2} m
Q_a =10^5 J mol^{-1}
Q_b = 10^5 J mol^{-1}
ρ_s=2.6·10^3 kg m^{-3}
ρ_w=10^3 kg m^{-3}
C_s=1000 J kg^{-1} K^{-1}
C_w=4186 J kg^{-1} K^{-1}
K_s=2.6 W $m^{-1}K^{-1}$
K_w=0.603 W $m^{-1}K^{-1}$
ϕ=0.1
η= 10^{-6} m^2 s^{-1}
V_0= 3.5 cm yr^{-1}
γ=1.14· 10^{-3} Pa s